# Effect of β-Crystals on the Mechanical and Electrical Properties of β-Nucleated Isotactic Polypropylene

**Wei Zhang[1], Man Xu[1], Kaiwen Huang[1], Qiulin Mu[1]** and **George Chen[1,2]**
[1]State Key Laboratory of Electrical Insulation and Power Equipment
Xi'an Jiaotong University
Xi'an, 710049, China
[2]School of Electronics and Computer Science
University of Southampton
Southampton, SO17 1BJ, UK

## ABSTRACT

**Polypropylene has great potential as a thermoplastic insulation material for high voltage direct current (HVDC) cable. However, its mechanical properties restrict its application, particularly at low temperature. In this paper, isotactic polypropylene (iPP) with the β-nucleating agent WBG was prepared by the melt blending method. The crystallinity, β-crystal proportion and crystalline morphology were analyzed by wide-angle X-ray diffraction, differential scanning calorimetry, scanning electron microscopy and polarized optical microscopy. The results showed that the crystallinity and β-crystal proportion increased as the WBG concentration increased. Three types of β-crystal morphology, namely β-spherulite, flower-like agglomerate and β-quasi-spherulite, were sequentially obtained with increasing WBG concentration. The mechanical properties, space charge distribution, thermally stimulated discharge current and DC electrical breakdown strength were investigated. Compared with pure iPP, the Izod impact strength and DC breakdown strength of iPP/0.1%WBG were improved by 238% and 16%, respectively, and the fracture energy and brittleness temperature of iPP/0.3%WBG were improved by 420% and 80%, respectively. In addition, the space charge accumulation was suppressed in the range of 0.1-0.5 wt% WBG. Chain coupling between the β-crystals and the amorphous phase, particularly in the flower-like agglomerates, was considered to play an important role in improving the mechanical and electrical performance.**

Index Terms —**polypropylene, β-crystal, mechanical property, DC electrical property**

## 1 INTRODUCTION

The increasing demand for renewable energy and long distance power transmission has promoted the development of high voltage direct current (HVDC) transmission technology, and the voltage sourced converter (VSC) HVDC system based on extruded cables has become the primary choice in underground and off-shore power transmission [1]. At the present stage, most commissioned VSC-HVDC cable systems are constructed with cross-linked polyethylene (XLPE) insulated cables. However, the manufacturing process of XLPE produces cross-linking byproducts, resulting in space charge accumulation in the insulation. The presence of the space charge can distort the electric field distribution and affect the electrical performance of XLPE HVDC cables. Additionally, after the retirement of the cables, it is difficult to recycle XLPE. With the growing awareness of environmental protection among the public, the identification of renewable insulating materials has become an active research topic in the dielectric community. Isotactic polypropylene (iPP) is a nonpolar material with a low dielectric constant and high insulation resistivity and is recyclable. iPP has sufficient mechanical properties at high temperatures and can be operated at temperatures exceeding 90 °C [2, 3]. The manufacturing of iPP employs simple processing technology without a cross-linking procedure, which not only greatly reduces the production period but also helps suppress the accumulation of space charge. Based on these advantages, iPP is a potential alternative for HVDC cable insulation [4].

*Manuscript received on 28 June 2018, in final form XX Month 20xx, accepted xx Month 20xx. Corresponding author: M. Xu.*

However, the low fracture toughness and low impact resistance of iPP limit its application as an insulating material for power cables. Blending iPP with other thermoplastic polyolefins (TPOs) can improve its flexibility, but space charge accumulates in the blends because of the discontinuity between the iPP and TPOs [5, 6]. In addition, the long-term stability of the two-phase material requires further study. Doping nanofiller in the PP matrix could suppress the accumulation of space charge, but the agglomeration of nanofillers introduces many problems, such as interrupting the continuous extrusion of cable [7, 8]. Compared with adding new ingredients by blending and doping, adjusting the supermolecular structure of the iPP by changing the crystalline forms leads to significant improvements in mechanical and thermal properties [9]. iPP is a semicrystalline polymer that can crystallize in several crystalline forms: monoclinic α-crystals, trigonal β-crystals, orthorhombic γ-crystals, etc. However, iPP mostly appears as α-crystals if no special treatment is adopted.

In recent years, an increasing number of studies have sought to improve the properties of iPP by introducing β–crystals. Chen et al [10] and Wu et al [11] found that the formation of large amounts of β-crystal in iPP improved fracture resistance. Raab et al [12] and Kotek et al [13] found that β-crystals decreased the Young's modulus and yield stress and increased the fracture energy. Lv et al [14] reported that β-crystal iPP exhibited higher oxidation stability than α-crystal iPP. Because of the mechanical and thermal advantages of β-crystals, it is possible to use β-crystals to improve the properties of polypropylene-based insulating material for high voltage cable. Our previous studies have revealed that the electrical breakdown strength and resistivity stability at high temperatures of iPP were improved by introducing β-crystals [15]. iPP with β-crystals is considered potentially suitable for HVDC cable insulation [16] because of its low space charge injection and high DC breakdown strength [17]. These studies show that the excellent electrical and mechanical properties are mainly attributable to the morphology of the β-crystals in iPP. The mechanism underlying these reported experimental results could be further elucidated by investigating the formation process and morphological characteristics of β-crystals in iPP.

In this paper, the β-nucleating agent WBG was selected to introduce β-crystals in the iPP matrix. Adding β-nucleating agent is one reliable means of introducing β-crystals. In addition, adding a β-nucleating agent reduces the temperature dependence of the crystallization process. A rapid cooling molding process was used to prepare the samples to improve the mechanical and electrical properties of the iPP matrix [3, 15]. Then, the influence of the WBG concentration on the crystallinity, β-crystal proportion and crystalline morphology was analyzed. The mechanical and DC electrical properties were investigated, and the mechanisms are discussed.

# 2 EXPERIMENTAL DETAILS

## 2.1 MATERIALS

Isotactic polypropylene (T30-S) with a density of 0.91 kg/L was provided by Shaanxi Yanchang Coal Yulin Energy and Chemical Co., Ltd. China. The β-nucleating agent WBG was provided by Winner Functional Materials Co. (Foshan, China).

## 2.2 BLENDING AND SAMPLE PREPARATION

First, the iPP pellets and WBG were mixed in a weight ratio of 95:5 and melt blended for master batch preparation in a micro twin-screw extruder (Thermo Haake, Process 11, Φ=11 mm, L/D=40). Second, the β-nucleated iPP was prepared in master batches and pure iPP pellets. The concentrations of WBG were 0.05, 0.1, 0.3, 0.5 and 1 wt%. The pure iPP were extruded for comparison. The screw speed was 300 rpm, the six temperature zones were 190, 200, 200, 200, 200, 200, and 200 °C, and the extrusion die head temperature was 200 °C.

At 240 °C, the pellets were heated in a stainless steel mold for 5 min and then compressively molded under 5 MPa in the vulcanizing machine. The molded samples were then moved to a water-cooled flat vulcanizing machine under 15 MPa until reached ambient temperature. The cooled rate was estimated to be 40-60 °C/min. The plate samples were used for mechanical and electrical tests.

## 2.3 CHARACTERIZATION

Crystalline structures of the samples were characterized by wide-angle X-ray diffraction (WAXD) using Cu-Ka radiation (Bruker, D8 ADVANCE). The data were collected at a scanning rate of 6 °/min.

Differential scanning calorimetry (DSC) measurements were performed by a DSC 822e (METTLER TOLEDO) instrument under nitrogen atmosphere. Each sample weighing approximately 5 mg taken from the prepared plate sample was heated to 240 °C and held for 5 min. Then, the samples were cooled to 30 °C and re-heated to 240 °C. The heating and cooling rate was 10 °C/min.

Scanning electron microscopy (SEM) measurements were performed using a VE-9800S SEM instrument to inspect the cryofractured surface of plate samples etched by permanganate solution [18]. The samples were coated with gold and observed under an acceleration voltage of 20 kV.

Morphological observations were performed by polarized optical microscopy (POM) (Olympus bx51-P) equipped with a Linkam THMS 600 hot stage under a crossed polarizer. The samples were melted at 240 °C and held for 5 min. Subsequently, the morphological photographs of crystallization were recorded with the aid of a digital camera during the cooled down period at 2 °C/min.

Tensile testing was undertaken at room temperature using a CMT-4503 mechanical tensile machine (Meitesi Industry System, China) at a fixed speed of 100 mm/min. For each sample, the tensile test was repeated five times.

The notched Izod impact strength of the samples was tested with a VJ-40 Izod machine according to the ISO 180: 2000 standard. The average value was obtained from five tests for each type of sample at room temperature.

The brittleness temperature of the samples was tested with a low-temperature embrittlement impact testing machine for plastics (DC2, Changshu CSET Corp., China). The tests were performed according to the ISO 974:2000 standard.

The trap level profiles in the samples were calculated by the thermally stimulated depolarization current (TSDC) method [19]. The sample was first polarized at 50 °C with a positive DC electric field of 3 kV/mm for 20 min and then cooled at a rate of 30 °C/min. When the temperature was -100 °C, the poling voltage was moved, and the sample was shorted for 5 min. The depolarization current was measured from -100 to 100 °C at a heating rate of 3 °C/min.

The space charge behavior of the samples was measured using the pulsed-electro-acoustic (PEA) method at room temperature. An electric field of 50 kV/mm was applied to the samples for 1800 s. The space charge profiles were recorded at various times for analysis. The electrode materials were carbon black-filled polymer (anode) and Al (cathode).

The DC breakdown strength was measured using a DC dielectric strength tester (ZGF-200 kV/5 mA, Shanghai Welldone Corp., China) with 25-mm-diameter sphere copper electrodes. Samples with an average thickness of 200 μm were placed between the electrodes and immersed in vegetable oil. A 2 kV/s ramping voltage was applied until breakdown at room temperature. The results from 20 tests for each type of sample were analyzed assuming Weibull distribution.

## 3 RESULTS AND DISCUSSION

### 3.1 CRYSTAL STRUCTURE

WAXD was used to quantitatively estimate the β-crystalline proportion ($K_\beta$) and crystallinity ($X_c$) of the plate samples. Figure 1 shows that the characteristic diffraction peaks of pure iPP are at 2θ=14.2°, 17.1°, 18.6°, and 21.9°, which correspond to the α (110), α (040), α (130) and α (111) planes, respectively, indicating that only α-crystals exist in pure iPP [14]. However, for the β-nucleated iPP, the diffraction peak at 2θ=16.2° corresponds to β (300), indicating the appearance of β-crystals in iPP. According to the Turner-Jones equation [20], the $K_\beta$ and $X_c$ values obtained by the calculation from the WAXD profiles are shown in Table 1.

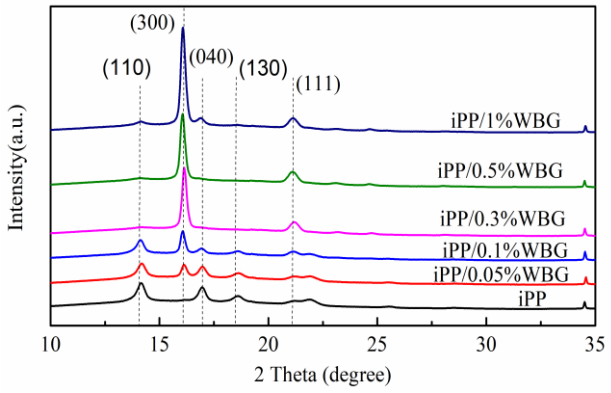


**Figure 1**. WAXD spectra of iPP containing various WBG concentrations.

**Table 1.** Crystallinity data of iPP containing various WBG concentrations.

| Samples | WAXD | | DSC | | | |
|---|---|---|---|---|---|---|
| | $K_\beta$ (%) | $X_c$ (%) | $T_{m\beta}$ (℃) | $T_{m\alpha}$ (℃) | $X_{m\beta}$ (%) | $X_{m\alpha}$ (%) |
| iPP | / | 50.8 | / | 165.8 | / | 38.6 |
| iPP/0.05%WBG | 40.1 | 53.0 | 148.3 | 163.8 | 13.5 | 30.1 |
| iPP/0.1%WBG | 59.7 | 55.2 | 151.5 | 166.6 | 30.0 | 18.1 |
| iPP/0.3%WBG | 75.7 | 54.2 | 150.9 | 168.3 | 32.6 | 17.0 |
| iPP/0.5%WBG | 79.7 | 55.8 | 152.3 | 168.3 | 36.3 | 10.8 |
| iPP/1%WBG | 80.1 | 56.3 | 153.1 | 168.0 | 37.3 | 7.9 |

The WAXD results show that the $X_c$ of pure iPP is 50.8%, while the $X_c$ of the β-nucleated iPP is higher than that of pure iPP. The $K_\beta$ of iPP/0.05%WBG is 40.1%, and the $K_\beta$ of iPP/0.5%WBG is approximately 79.7%. The $K_\beta$ and $X_c$ values are 80.1% and 56.3% for iPP/1%WBG, indicating that $K_\beta$ tends toward saturation. The addition of WBG induces the generation of β-crystals and increases the crystallinity.

DSC was adopted to analyze the nonisothermal crystallization behaviors. As shown in Figure 2, the 1st run curve is the melting curve of the plate samples; the 2nd run curve is the melting curve of the same sample that crystallized in the DSC instrument with a cooling rate of 10 °C/min. The crystallinity was calculated by dividing the enthalpies of fusion calculated from the DSC curves by the melt enthalpy values of α- and β-crystal of completely crystallized polypropylene, which are 177.0 and 168.5 J/g, respectively [21]. The melting temperature ($T_{m\beta}$, $T_{m\alpha}$) and crystallinity of the β- and α-crystals ($X_{m\beta}$, $X_{m\alpha}$) from the 2nd run curve are shown in Table 1.

In both runs, pure iPP had one melting peak corresponding to α-crystal. For the β-nucleated iPP, the 1st run exhibited three endothermic melting peaks. The melting peak at the highest temperature is associated with α-crystal. The middle peak at 150.6-153.2 °C is the characteristic melting temperature of β-crystal. The melting peaks located at 142.7-148.6 °C represent the metastable β-crystals. The 2nd run curves of the β-nucleated iPP samples had two melting peaks; the peak at higher temperature still represents α-crystal, whereas the peak at lower temperature (148.3-153.1 °C) represents β-crystal, which was transformed from two β-crystal peaks in the 1st run. In both runs, the area of the β-crystal increased as the WBG concentration increased, indicating that the β-crystallinity increased as WBG increased.

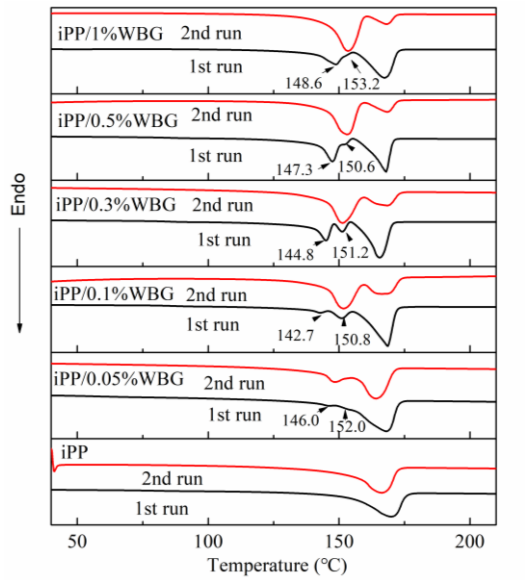


**Figure 2**. The DSC melting traces (1st and 2nd melting runs) for iPP containing various WBG concentrations.

These results show that a lower cooling rate can assist the formation and growth of β-crystals and eliminate imperfect β-crystals. When the cooling rate was 40-60 °C/min, the samples rapidly enter the low-temperature region, and the molecular chain of iPP folded into self-nuclei in the low-temperature region; consequently, more α-crystals were observed in the plate samples. As the cooling rate decreased, WBG provided a large number of heterogeneous nuclei that induced β-crystal formation, and thus crystallization occurred in the high-temperature region. The β-crystals introduced by WBG decreased the proportion of α-crystals. For the α-crystal melting peak, the area of the 2nd curve was smaller than that of the 1st run. At a slow cooling rate, $X_{m\beta}$ increased as the WBG concentration increased, but the value of $X_{m\alpha}$ did not increase. In conclusion, the effective combination of the WBG concentration and cooling rate enabled increased formation of β-crystals. The effects of different crystallization conditions and the annealing process on the electrical and mechanical properties are evaluating and will be reported later.

### 3.2 MORPHOLOGICAL OBSERVATIONS

For the plate samples, the morphologies of the crystals were observed by SEM. As shown in Figure 3 (a), α-spherulites were observed in pure iPP. Mixed α- and β-spherulites were observed in iPP/0.05%WBG (Figure 3 (b)), and flower-like agglomerates of β-crystals were observed in iPP/0.1%WBG, iPP/0.3%WBG and iPP/0.5%WBG, as shown in Figure 3 (c) (d) (e). The diameter of the flower–like agglomerates increased as the WBG increased. Large amounts of β-quasi-spherulites were observed in iPP/1%WBG, as shown in Figure 3 (f) (f'). In pure iPP, the α-spherulites had clear boundaries, but chain coupling between the β-crystals and the amorphous phase was observed in the β-nucleated iPP samples. The diameters of the α-spherulites, β-spherulites and flower–like agglomerates are listed in Table 2.

**Table 2.** Diameters of α- and β-crystals for various β-nucleated iPP.

| Samples | α-crystal (μm) | β-crystal (μm) |
|---|---|---|
| iPP | 23.4 | / |
| iPP/0.05%WBG | 15.5 | 21.5 |
| iPP/0.1%WBG | 8.9 | 21.2 |
| iPP/0.3%WBG | 4.4 | 25.6 |
| iPP/0.5%WBG | 5.3 | 38.8 |
| iPP/1%WBG | / | 1.5 |

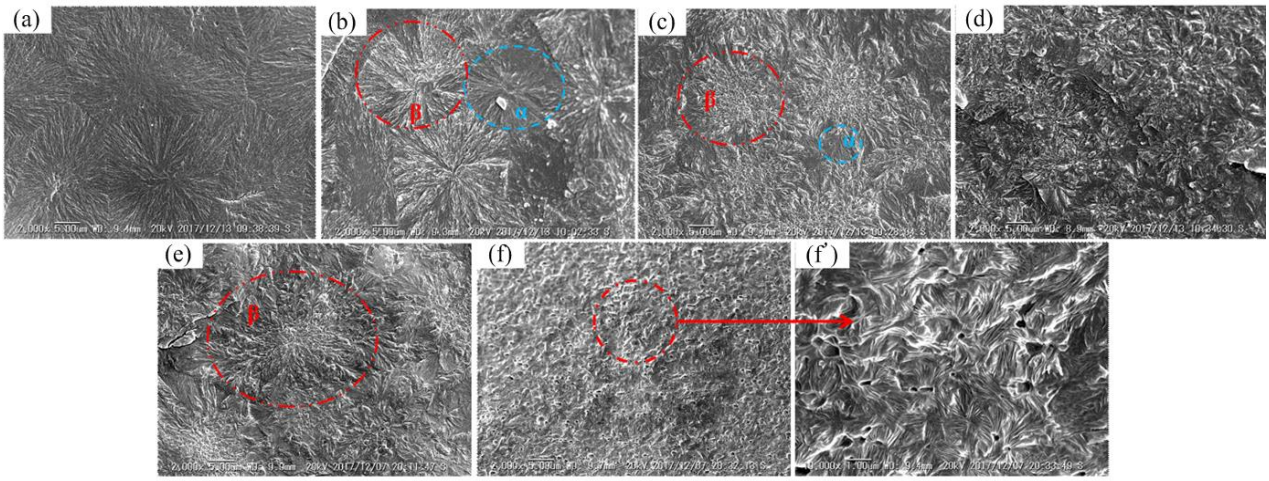


**Figure 3.** SEM photographs of iPP containing various WBG concentrations: (a) pure iPP, (b) 0.05 wt%, (c) 0.1 wt%, (d) 0.3 wt%, (e) 0.5 wt%, (f, f') l wt%.

For comparison, the WBG concentrations on the supermolecular of iPP containing various WBG samples were observed by POM. As shown in Figure 4, the nucleation process and crystal growth pattern of WBG containing iPP differed from those of pure iPP. Pure iPP folded into self-nuclei at approximately 130 °C and grew into α-spherulites with an obvious Maltese cross at approximately 120 °C [9]. When the temperature decreased to 115 °C, α-spherulites with clear boundaries stopped growing, and their average diameter was approximately 200 μm, as shown in Figure 4 (a4).

In the low WBG concentration regimes (below 0.1 wt%), the tiny granules of WBG dissolved in iPP, as shown in Figure 4 (b1). The β-crystals appear brighter than the α-

crystals because of their very strong negative birefringence [9]. When cooled to 132 °C, the birefringent crystal induced on the surface of WBG was β-crystal. At approximately 130 °C, α-nuclei began to grow, which are evident as the darker crystal in Figure 4 (b3). As the temperature decreased, the diameters of the α- and β-spherulites increased simultaneously. Finally (Figure 4 (b4)), the average diameter of the α- and β-spherulites was approximately 100 μm.

At moderate WBG concentrations (0.1-0.5 wt%), the WBG built complex network structures via recrystallization and self-organization before iPP crystallization (Figure 4 (c1, d1 and e1)). The β-crystals grew along the self-organized WBG network at approximately 132 °C, and α-spherulites began to grow at the same time. At approximately 130 °C, the birefringent β-crystals grouped into a large flower-like agglomerate, as shown in Figure 4 (c3, d3 and e3). At the end of crystallization, the diameter of the flower increased as the WBG concentration increased; the average diameter of the flower-like agglomerates was 200 μm in iPP/0.1%WBG and 300 μm in iPP/0.5%WBG. However, at a high concentration of WBG (1 wt%), because of the steric restriction of propagation, most of the WBG could not be dissolved in the samples. Therefore, large amounts of β-quasi-spherulite were formed in the iPP/1%WBG sample, as shown in Figure 4 (f4).

The final crystallization images of POM is similar with the results of SEM, but the diameters of α- and β-crystals observed by SEM were smaller than those observed by POM. This discrepancy occurred because the cooling rate of the plate samples was too rapid for crystal growth. However, the trends of the change in crystalline morphology with WBG concentration were similar at both the fast and slow cooling rates. Fast and slow cooling can produce similar supermolecular structures at the same WBG concentration. Therefore, the crystal structure can be adjusted by controlling the WBG concentration. In addition, the mechanical and electrical properties of the samples obtained with a fast cooling rate discussed below can be explained by the conclusions of the structural analysis.

As shown in the POM images, α- and β-crystals coexisted in the samples of WBG containing iPP, which indicates that WBG showed dual selectivity to α- and β-crystals. The α-crystals had clear boundaries, whereas the β-crystals had irregular and fuzzy boundaries. These results agree with those obtained by WAXD and DSC.

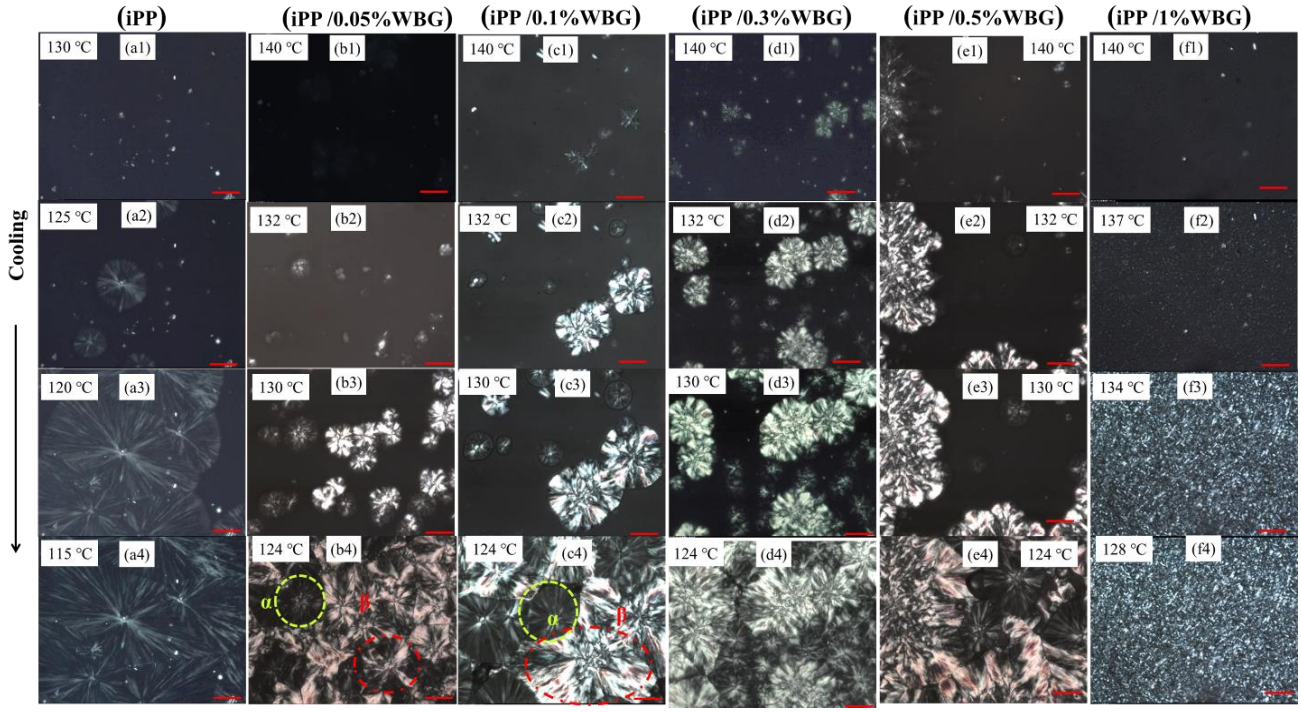


**Figure 4.** Typical POM images representing the crystallization process of iPP containing various WBG concentrations: (a) pure iPP, (b) 0.05 wt%, (c) 0.1 wt%, (d) 0.3 wt%, (e) 0.5 wt%, (f) l wt%. Scale bars represent 50 μm.

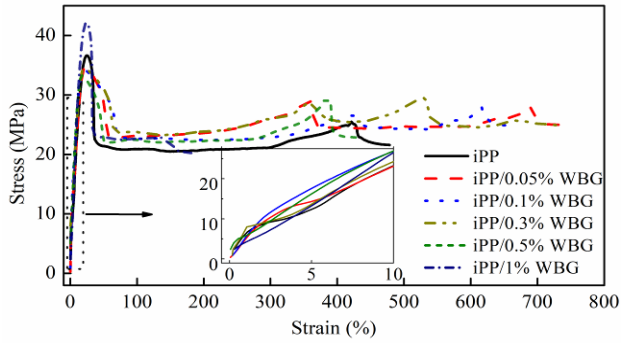


**Figure 5.** Tensile stress-strain curves of various β-nucleated iPP.

**Table 3.** Mechanical properties of various β-nucleated iPP

| Samples | Tensile Strength (MPa) | Elongation (%) | Fracture Energy (kJ/m²) | Izod impact strength (kJ/m²) | Brittleness temperature (°C) |
|---|---|---|---|---|---|
| iPP | 38.1±1.0 | 467.1±17.5 | 2.8±0.3 | 2.1±0.6 | -5.0 |
| iPP/0.05%WBG | 37.5±3.5 | 719.6±47.0 | 14.2±0.7 | 5.2±0.8 | -6.7 |
| iPP/0.1%WBG | 41.9±1.2 | 667.0±15.1 | 13.9±0.2 | 7.3±0.4 | -8.7 |
| iPP/0.3%WBG | 35.5±2.4 | 717.3±57.0 | 14.5±1.1 | 6.2±0.6 | -9.0 |
| iPP/0.5%WBG | 35.7±1.3 | 410.9±54.3 | 8.8±1.1 | 4.5±1.1 | -5.3 |
| iPP/1%WBG | 35.8±1.4 | 354.1±24.1 | 5.6±1.2 | 3.2±0.5 | -4.0 |

investigate the effects of various WBG concentrations on the mechanical properties. Typical tensile stress-strain curves are shown in Figure 5, and the values of tensile strength, elongation at break, fracture energy and Izod impact strength as well as brittleness temperature are summarized in Table 3.

As shown in Figure 5, all samples broke down after experiencing yield, which indicates the addition of WBG did not affect the tensile behavior of iPP. From the data in Table 3, it can be concluded that adding WBG will increase the elongation, fracture energy, Izod impact strength and brittleness temperature. Specifically for iPP/0.1%WBG, the fracture energy increased nearly 5 times, and the Izod impact strength increased more than 3 times. The brittleness temperatures of iPP/0.3%WBG was -4 °C lower than that of pure iPP. Thus, β-crystal improved the mechanical properties not only at normal temperature but also at low temperature. However, when the WBG concentrations were 0.5 wt% and 1 wt%, the mechanical properties began to decrease, and some values were even lower than those of pure iPP, such as elongation at break, tensile strength and brittleness temperature.

The improved toughness of the β-crystals can be explained by the following two factors. First, the mechanical load induces the transition of β-crystals to α-crystals, and the whole process absorbs energy and hinders mechanical failure [22]. Second, the chain coupling between the β-crystals and the amorphous phase is weaker than that between the α-crystals and the amorphous phase, which provides buffering and increases the toughness of the samples [9]. When the WBG content ranged from 0.1 to 0.5 wt%, the β-crystals agglomerated into large flower-like structures, as observed by POM and SEM. This structure possesses more interfaces between the crystals and the amorphous phase. In iPP/0.5%WBG, the diameter of the flower-like agglomerates was larger, and thus few couplings formed between the flower-like agglomerates and the amorphous phase, thus decreasing the elongation at break, Izod impact strength and brittleness temperature. At the highest concentration of 1 wt% WBG, coupling between the spherulites and the amorphous phase barely existed for most of the β-quasi-spherulites. Although the values of $K_\beta$ and $X_c$ of iPP/1%WBG were high, the elongation at break, tensile strength and brittleness temperature were lower than those of pure iPP. Thus, the mechanical properties of WBG containing iPP were affected by not only the β-crystal proportion but also the β-crystal morphology. Simply increasing the concentration of WBG will not monotonically improve the mechanical properties of iPP.

### 3.4 TRAP CHARACTERISTICS

Based on TSDC theory [19], the trap level distribution can be calculated from the TSDC spectrum. The trap distributions of iPP containing various WBG concentrations are shown in Figure 6 and Table 4.

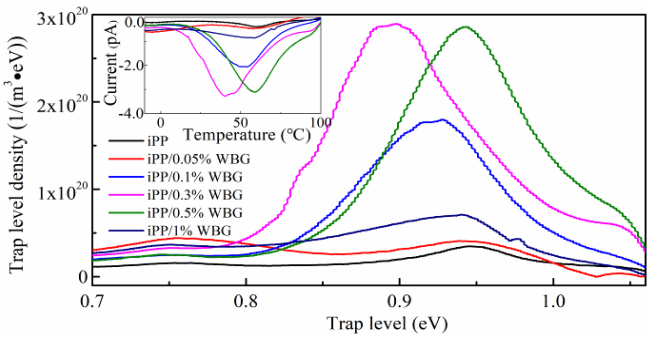


**Figure 6**. Trap level distribution of various β-nucleated iPP; inset, the thermally stimulated current spectrum

The results show that the trap levels of all samples ranged from 0.9-0.94 eV, which are regarded as deep traps in iPP. The deep traps exist between the crystals and the amorphous phase. As shown in Table 4, when the WBG concentration was less than 0.5 wt%, the trap level density increased as $K_\beta$ increased. The weak coupling between the β-crystals and amorphous phases induced more deep traps. For iPP/0.5%WBG, the trap level density did not increase because the diameter of the flower-like agglomerates was too large, and thus the number of couplings between the β-crystals and amorphous phase did not increase. When the WBG concentration was 1 wt%, the large amounts of small β-quasi-spherulites resulted in a lack of coupling between the spherulites and the amorphous phase. Thus, even though the $K_\beta$ of iPP/1%WBG was 80.1%, the deep trap density decreased to $7.1\times10^{19}$ $m^{-3}\cdot eV^{-1}$.

**Table 4.** Trap level and trap level density of various β-nucleated iPP.

| Samples | Trap level (eV) | Trap level density×$10^{19}$ ($m^{-3}\cdot eV^{-1}$) |
|---|---|---|
| iPP | 0.94 | 3.3 |
| iPP/0.05%WBG | 0.94 | 4.0 |
| iPP/0.1%WBG | 0.92 | 17.7 |
| iPP/0.3%WBG | 0.90 | 28.4 |
| iPP/0.5%WBG | 0.94 | 28.4 |
| iPP/1%WBG | 0.94 | 7.1 |

### 3.5 SPACE CHARGE BEHAVIOR

The space charge is one of the most important factors for evaluating the properties of insulating materials for HVDC cables. Figure 7 describes the space charge accumulation and electric field distribution during polarization in samples subjected to a DC electric field of 50 kV/mm for 1800 s.

As shown in Figure 7 (a1), a large amount of heterocharge accumulated near the anode and cathode over time. The corresponding electric field was enhanced to approximately 60 kV/mm after 1800 s, as shown in Figure 7 (a2). In iPP/0.05%WBG, as shown in Figure 7 (b1), the heterocharge accumulation near the cathode was slightly reduced, and the largest electric field distortion was only 5 kV/mm. Almost no space charge accumulated in the iPP/0.1%WBG, iPP/0.3%WBG and iPP/0.5%WBG samples, and thus there was no obvious electric field distortion, as shown in Figure 7 (c2), (d2) and (e2). For iPP/1%WBG, as shown in Figure 7

(f1), a small amount of heterocharge accumulated near the anode and the cathode. Figure 7 (f2) shows that the electric field at the position of the heterocharge reached 55.3 kV/mm, resulting in a field distortion of 10.6%.

Taken together, the space charge and electric field distribution results showed that the flower-like agglomerates have excellent space charge suppression characteristic. The space charge is considered to be closely related to carrier traps. The flower-like agglomerates had more traps at the couplings between the interface of the β-crystals and amorphous phase, as proven by TSDC and SEM. The deep traps at the couplings capture carriers (e.g., electrons and/or holes) to prevent charge transport [23]. Therefore, the space charges in the iPP/0.1%WBG, iPP/0.3%WBG and iPP/0.5%WBG samples were remarkably suppressed, and the electric field distributions were more uniform, which is beneficial for improving the DC breakdown strength.

### 3.6 DC BREAKDOWN STRENGTH

The DC breakdown strength is one of the key factors determining the voltage level of HVDC cable. The Weibull plots of DC breakdown strength and the characteristic breakdown strength ($E_0$) and shape parameter ($B$) are given in Figure 8. The $E_0$ of pure iPP was 389.0 kV/mm, lower than that of β-nucleated iPP. For iPP/0.1%WBG and iPP/0.3%WBG, the $E_0$ was 449.3 and 436.4 kV/mm, 16 and 12 % higher than that of pure iPP, respectively.

The short time for electrical breakdown is influenced by the amount of free electrons and the energy of free electrons gained in the electric field. In the β-nucleated iPP samples, free electrons were captured by the deep traps between the β-crystals and amorphous phases, leading to a decrease in the amount of free electrons. At the same time, the inversion electric field induced by the heterocharge that accumulated near the electrodes not only acted as the neutralization center for the electrons but also reduced the average electric field strength in the sample. These factors account for the increment of the breakdown strength [24].

The shape parameter $B$ is affected by the crystal size and the coupling between the crystal and amorphous phases. The $B$ of pure iPP was 7.9 because of the lack of coupling, and the $B$ of β-nucleated iPP was higher. For iPP/1%WBG, $B$ was 12.9 due to the uniform size of the β-quasi-spherulite.

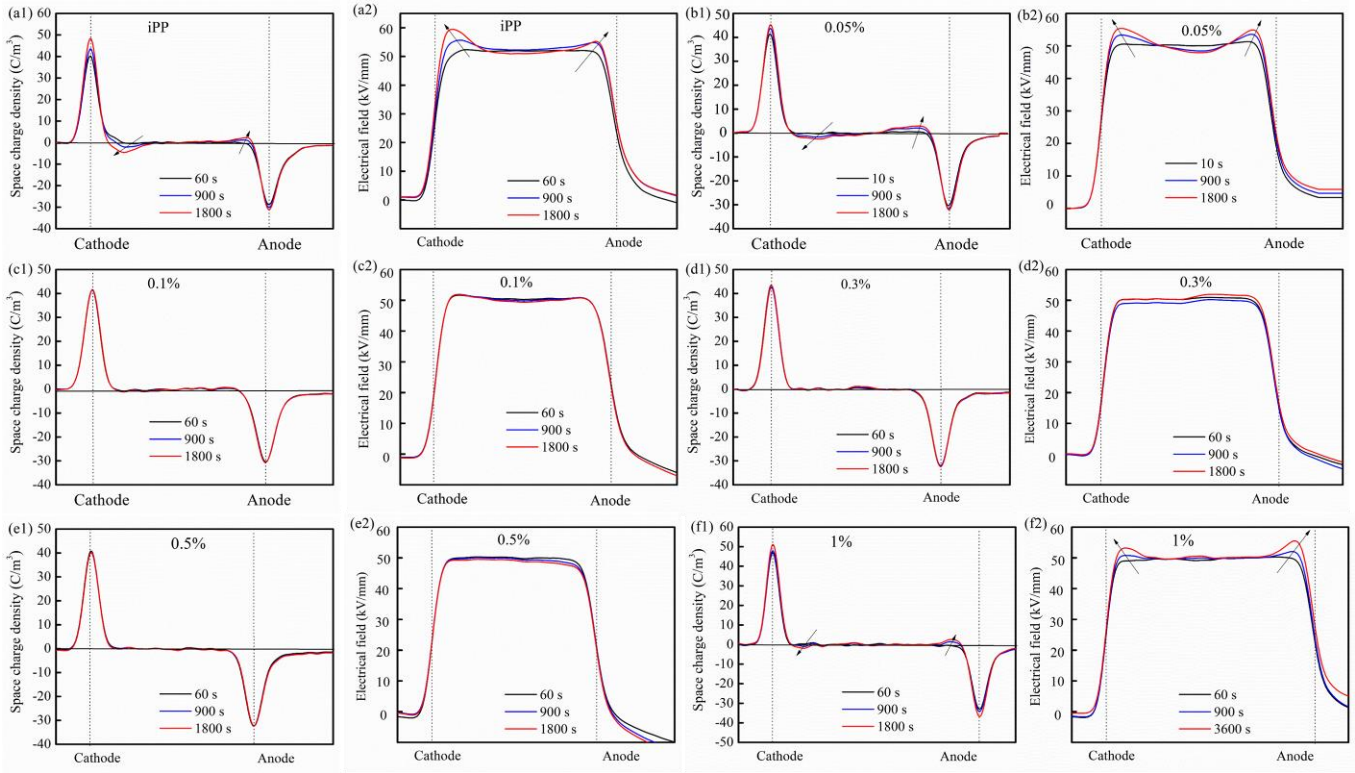


**Figure 7.** Space charge (1) and electric field (2) distribution during polarization in (a) iPP, (b) 0.05 wt%, (c)0.1 wt%, (d) 0.3 wt%, (e) 0.5 wt%, (f) 1 wt%

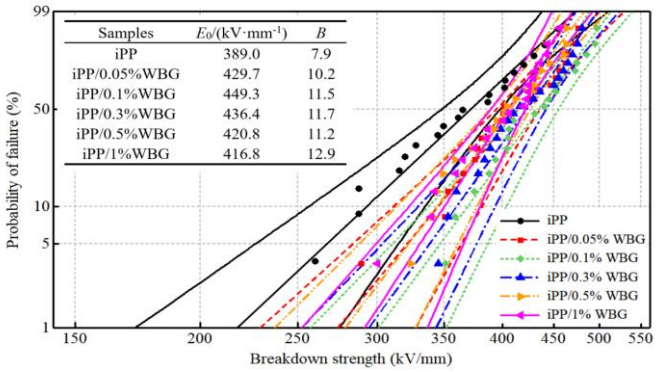


**Figure 8.** Weibull plots and 95% confidence interval of DC breakdown strength of various β-nucleated iPP

## 4 CONCLUSION

In this study, the effects of the WBG concentration on the β-crystal proportion, crystal morphology, mechanical and electrical properties of various β-nucleated iPP samples were investigated in detail.

The β-nucleating agent WBG and iPP were prepared by melt blending to introduce β-crystals in iPP. The crystallinity and β-crystal proportion increased as the WBG concentration increased. In the high WBG concentration regimes (above 0.3 wt%), the crystallinity was greater than 54%, and the β-crystal proportion was greater than 75%, tending toward saturation. The self-organization and recrystallization behaviors of WBG played important roles in determining the final crystalline morphology in iPP. Three types of β-crystal morphology, β-spherulite, flower-like agglomerate and β-quasi-spherulite, were sequentially obtained with the increment of WBG concentration. A lower cooling rate was favorable for growing large, well formed β-crystals. The trends of the crystalline morphology change were similar at fast and slow cooling rates.

At WBG concentrations of less than 0.3 wt%, Izod impact strength and fracture energy were approximately 3 and 7 times higher than those of pure iPP, respectively. Meanwhile, the brittleness temperature was nearly 80% lower than that of pure iPP. The DC breakdown strength was 449.3 kV/mm, 16% higher than that of pure iPP. In the range of 0.1-0.5 wt% WBG, the space charge accumulation was suppressed remarkably due to the large amount of deep traps. These improvements in mechanical and electrical properties can be attributed to the increase in the β-crystal proportion and chain coupling between the β-crystals and the amorphous phase.

## 5 ACKNOWLEDGMENTS

This work was financially supported by National Key Research and Development Program of China (2016YFB0900702).

## REFERENCES

[1] G. Chen, M. Hao, Z. Xu, A. Vaughan, J. Cao, and H. Wang, "Review of high voltage direct current cables," CSEE Journal of Power and Energy Systems, vol. 1, no. 2, pp. 9-21, May. 2015.

[2] C. D. Green, A. S. Vaughan and G. C. Stevens, "Thermoplastic Cable Insulation Comprising a Blend of Isotactic Polypropylene and a Propylene-ethylene Copolymer," IEEE Trans. Dielectr. Electr. Insul., vol. 22, no. 2, pp. 639-648, Apr. 2015.

[3] I. L. Hosier, A. S. Vaughan and S. G. Swingler, "An investigation of the potential of polypropylene and its blends for use in recyclable high voltage cable insulation systems," J. Master. Sci., vol. 46, no. 11, pp. 4058-4070, Feb. 2011.

[4] W. Zhang, M. Xu, G. Cheng, M. L. Fu, S. Hou and W. K. Li, "Structure and Properties of Isotactic Polypropylene and Ethylene-propylene Copolymer," High Voltage Engineering, vol. 43, no. 11, pp. 3634-3644, Nov. 2017.

[5] I. L. Hosier, L. Cozzarini, A. S. Vaughan and S. G. Swingler, "Propylene based systems for high voltage cable insulation applications," J. Phys.: Conf. Ser., vol. 183, no. 1, pp. 1-5, Jul. 2009.

[6] Y. Zhou, J. L. He, J. Hu, X. Y. Huang, and P. K. Jiang, "Evaluation of polypropylene/polyolefin elastomer blends for potential recyclable HVDC cable insulation applications," IEEE Trans. Dielectr. Electr. Insul., vol. 22, no. 2, pp. 673-681, Apr. 2015.

[7] K. Y. Lau, A. S. Vaughan and G. Chen, "Nanodielectrics: Opportunities and Challenges," IEEE Elect. Insul. Mag., vol. 31, no. 4, pp. 45-54, Aug. 2015.

[8] N. Fuse, Y. Ohki and T. Tanaka, "Comparison of nano-structuration effects in polypropylene among four typical dielectric properties," IEEE Trans. Dielectr. Electr. Insul., vol.17, no. 3, pp. 671-677, Jun. 2010.

[9] V. József, "β-modification of isotactic polypropylene: preparation, structure, processing, properties, and application," J. Macromol. Sci., vol. B41, no.4-6, pp. 1121-1171, Feb. 2002.

[10] H. B. Chen, J. K. Kocsis, J. S. Wu, and J. Varga, "Fracture toughness of α- and β-phase polypropylene homopolymers and random- and block-copolymers," Polym., vol. 43, no. 24, pp. 6505-6514, Nov. 2002.

[11] H. Y. Wu, X. X. Li, J. W. Chen, L. N. Shao, T. Huang, Y. Y. Shi, and Y. Wang, "Reinforcement and toughening of polypropylene/organic montmorillonite nanocomposite using β-nucleating agent and annealing," Compos. Part B: Engineer., vol. 44, no. 1, pp. 439-445, Apr. 2013.

[12] M. Raab, J. Ščudla and J. Kolařík, "The effect of specific nucleation on tensile mechanical behaviour of isotactic polypropylene," Eur. Polym. J., vol. 40, no. 7, pp. 1317-1323, Jul. 2004.

[13] J. Kotek, M. Raab, J. Baldrian, and W. Grellmann, "The effect of specific β-nucleation on morphology and mechanical behavior of isotactic polypropylene," J Appl. Polym. Sci., vol 85, no. 6, pp. 1174-1184, May. 2002.

[14] Y. D. Lv, Y. J. Huang, M. Q. Kong, and G.X. Li, "Improved thermal oxidation stability of polypropylene films in the presence of β-nucleating agent," Polym. T., vol. 32, no. 2, pp. 179-186, Apr. 2013.

[15] W. Zhang, M. Xu, M. X. He, G. Chen, and S. Hou, "Effect of the β-crystal formation in isotactic polypropylene used for eco-friendly insulating material," in IEEE *Int. Conf. Electr. Mater. Power Equipm.*, 2017, pp. 419-423.

[16] Y. H. Wu, J. W. Zha, W. K. Li, S. J. Wang, and Z. M. Dang, "A remarkable suppression on space charge in isotatic polypropylene by inducing the β-crystal formation," Appl. Phys. Lett., vol. 107, no. 11, pp. 112901, Sep. 2015.

[17] X. Y. Huang, Y. Y. Fan, J. Zhang and P. K. Jiang, "Polypropylene based thermoplastic polymers for potential recyclable HVDC cable insulation applications," IEEE Trans. Dielectr. Electr. Insul, vol. 24, no. 3, pp. 1446-1456, Jun. 2017.

[18] R. H. Olley and D. C. Bassett. "An improved permanganic etchant for polyolefines," Polym., vol. 23, no. 12, pp. 1707-1710, Jun. 1982.

[19] F. Q. Tian, W. B. Bu, L. S. Shi, C. Yang, Y. Wang, and Q. Q. Lei, "Theory of modified thermally stimulated current and direct determination of trap level distribution," J. Electrost., vol. 69, no. 1, pp. 7-10, Nov. 2011.

[20] A. T. Jones, J. M. Aizlewood and D. R. Beckett, "Crystalline forms of isotactic polypropylene," Macromol. Chem. Phys., vol. 75, no. 1, pp. 134-158, Oct. 1964.

[21] J. X. Li and W. L. Cheung. "Effect of mould temperature on the formation of α/β polypropylene blends in injection moulding," J. Mater. Process. Technol., vol. 1, no. 1, pp. 472-475, Jan. 1997.

[22] J. Kargerkocsis, "How does "phase transformation toughening" work in semicrystalline polymers?," Polym. Eng. Sci., vol. 36, no. 2, pp. 203-210, Jan. 1996.

[23] G. Mazzanti, G. C. Montanari and J. M. Alison, "A space-charge based method for the estimation of apparent mobility and trap depth as markers for insulation degradation-theoretical basis and experimental validation," IEEE Trans. Dielectr. Electr. Insul., vol. 8, no. 2, pp. 187-197, Apr. 2003.

[24] G. C. Montanari, “Bringing an insulation to failure: the role of space charge,” IEEE Trans. Dielectr. Electr. Insul, vol. 18, no. 2, pp. 339-364, Mar. 2011.

**Wei Zhang** was born in Heilongjiang, China, in 1989. She received a B.Sc. degree in electrical engineering from XiDian University, Xi’an, China, in 2011 and a M.Sc. degree in electrical engineering from Xi’an Jiaotong University, Xi’an, China, in 2013. Currently, she is a Ph.D. candidate in the Department of Electrical Engineering, Xi’an Jiaotong University. Her research interests include electrical insulation materials and high voltage engineering.

**Man Xu** (M’11) was born in Shaanxi, China, in 1977. She received B.S., M.S. and Ph.D. degrees in electrical engineering from Xi’an Jiaotong University, Xi’an, China, in 1999, 2002 and 2008, respectively. She subsequently became a lecturer at Xi’an Jiaotong University. She worked at Bologna University as a visiting researcher from Oct. 2010 to Sept. 2011. She has been an associate professor at Xi’an Jiaotong University since 2011. Her research interests include electrical insulation materials and nanodielectrics.

**George Chen** was born in China in 1961. He received BEng (1983) and MSc (1986) degrees in electrical engineering from Xi’an Jiaotong University, China. After he obtained a PhD degree (1990) from the University of Strathclyde, UK, for work on permanent changes in the electrical properties of irradiated low-density polyethylene, he joined the University of Southampton as a postdoctoral research fellow and subsequently became a senior research fellow. In 1997, he was appointed as a research lecturer and promoted to a reader in 2002. He is now professor of HV engineering at the University of Southampton and a visiting professor at Xi’an Jiaotong University. Over the years, he has developed a wide range of interests in HV engineering and electrical properties of materials and has published more than 300 papers.